Equation of State and Shear Strength at Multimegabar Pressures: Magnesium Oxide to 227 GPa

Thomas S. Duffy, Russell J. Hemley, and Ho-kwang Mao

Geophysical Laboratory and Center for High-Pressure Research, Carnegie Institution of Washington,
5251 Broad Branch Road, NW, Washington, DC 20015

The equation of state, elasticity, and shear strength of magnesium oxide were examined to 227 GPa using synchrotron x-ray diffraction in a diamond anvil cell. Static compression, ultrasonic elasticity, and shock data for MgO from ambient pressure to above 200 GPa can all be described by a single Birch-Murnaghan equation of state when the static shear strength, which is determined to be at least 11 GPa at 227 GPa, is taken into account. Our results show that there are significant changes in the degree and character of the elastic anisotropy of MgO at high pressure.

Understanding the physics of materials at ultrahigh pressure is an important focus of current work in condensed matter science. The equation of state (EOS) and phase stability are the most fundamental properties obtained from these investigations. The reliability of equation of state determinations at large compressions is uncertain because the stress state at multimegabar static pressures is not well understood [1,2]. Shear strength provides a fundamental description of a material's mechanical behavior, but little is known about this quantity under high static pressures [2,3]. Upon compression, the stress state of all solids is nonhydrostatic when the sample has finite strength. If uncorrected, the presence of shear stresses can lead to systematic errors in the resulting bulk modulus and its pressure derivative [4,5]. Shear strength effects can also introduce errors in measured pressures when secondary calibrants (e.g., ruby fluorescence or diffraction standards) are used [6]. As a result, there are typically discrepancies in equations of state determined by different techniques. In this study, we examine a low-Z prototype material (magnesium oxide) by x-ray diffraction at pressures above 200 GPa and provide the first determination of shear strength under such conditions. When this strength is taken into account, a single equation of state can describe ultrasonic, shock, and static compression data for this material. We show that it is possible to characterize material strength and elastic anisotropy at ultrahigh pressure directly from diffraction data.

Magnesium oxide is an ionic solid that has been widely studied at high pressure and is a prototype for developing and applying first-principles theoretical methods to oxides [7,8]. MgO has also been extensively employed in the development of experimental methods for shear strength determination at low pressures (to 40 GPa) [5,9,10]. A major problem with current data, however, is that equations of state from shock, ultrasonic, and static experiments are not mutually consistent [11]. Furthermore, theoretical models for MgO have been complicated by questions concerning the degree of ionicity and characterization of the charge distribution of the oxygen atoms [7,8].

Structural studies of materials at multimegabar pressures have largely been restricted to high atomic weight materials, due to the difficulty of performing x-ray diffraction on the extremely small volumes which can be subjected to such pressures. We show that with synchrotron radiation methods x-ray diffraction can be carried out on MgO, a low-Z oxide, to pressures in excess of 200 GPa. We also show that MgO remains in the $B1$ (NaCl) structure to these ultrahigh pressures, unlike other oxides which undergo pressure-induced phase transitions under moderate pressures [12].

MgO (99.998% purity) was mixed with 5 wt. % molybdenum and compressed in a Mao-Bell diamond anvil cell with beveled diamonds having central flats of 19.5 and 49.8 μm. Energy-dispersive synchrotron x-ray diffraction was carried out using superconducting wiggler radiation [13]. Figure 1 shows a representative x-ray diffraction pattern. For MgO, the (200), (220), and occasionally (420) peaks were resolved. Pressures were determined from Mo diffraction lines using an isotherm derived from shock data [14]. The pressure-volume relation is shown in Fig. 2. The range of stability
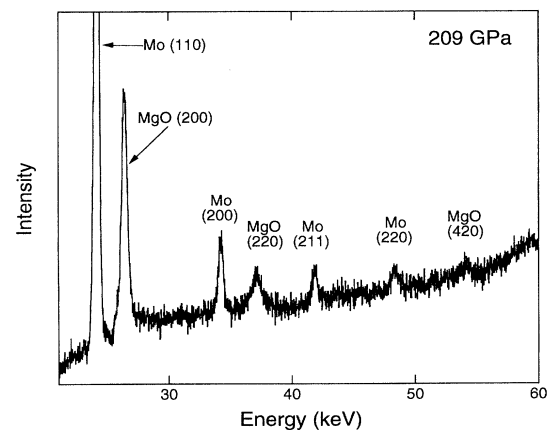

FIG. 1. Energy dispersive x-ray diffraction pattern of MgO at 209 GPa. The spectrum was taken in 150 min.
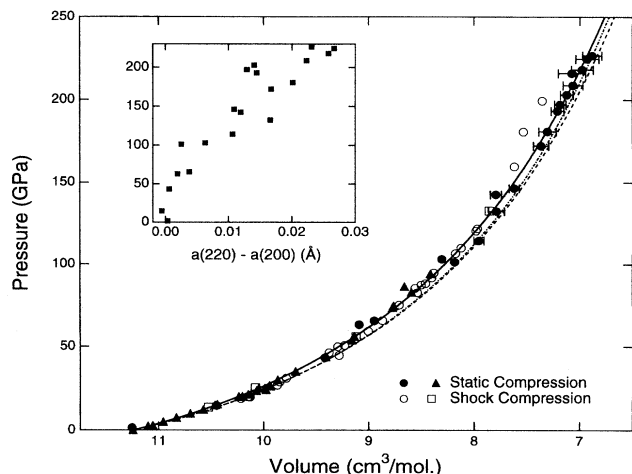
© 1995 The American Physical Society

FIG. 2. Pressure-volume data for MgO. The filled symbols are static compression data (circles—this study, triangles—[20]), and the open symbols are from shock compression (circles—single-crystal [16,17], squares—polycrystalline [18]). The solid line is a third-order Birch-Murnaghan fit to the present data. The dashed line is a third-order Birch-Murnaghan extrapolation of ultrasonic data. The dash-dotted line is a fourth-order Birch-Murnaghan fit to the combined ultrasonic and reduced shock data. The inset shows pressure versus the difference in the lattice parameters determined from the (220) and (200) diffraction lines.

predicted by theory for MgO in the $B1$ structure has varied widely (100–1000 GPa) (e.g., [7,8]). Our results show the $B1$ structure is stable to at least 227 GPa ($V/V_0 = 0.612$) at room temperature, demonstrating the remarkable stability range of MgO in this structure.

Ultrasonic sound velocity measurements [15] on MgO single crystals to 3 GPa yield high-precision values of the isothermal bulk modulus ($K_{0T} = 160.3 \pm 0.3$ GPa) and its first pressure derivative ($K_{0T}' = 4.15 \pm 0.10$). Using these parameters in a third-order Birch-Murnaghan equation yields the equation of state shown in Fig. 2. Shock compression data for MgO have been reported to 199 GPa [16–18]. At low pressures, where thermal effects are negligible, the single-crystal Hugoniot results are consistent with extrapolated ultrasonic data (Fig. 2). Mie-Grüneisen theory [16] was employed to reduce the shock data, and a Birch-Murnaghan equation fit to the resulting isotherm yields $K_{0T} = 157 \pm 7$ GPa and $K_{0T}' = 4.3 \pm 0.2$, in agreement with ultrasonic values. A combined fit to the reduced shock and ultrasonic data, in which K_{0T} and K_{0T}' are fixed, constrains the second pressure derivative of the bulk modulus, $K_{0T}'' = -0.022 \pm 0.004$ GPa^{-1}. This yields a fourth-order Birch-Murnaghan EOS which is slightly less compressible than the third-order fit (Fig. 2).

Recently, static compression data for MgO have been obtained to 23 GPa under quasihydrostatic conditions in the diamond cell using neon as a pressure medium and NaCl as an internal standard [19]. A third-order fit to these data yields $K_{0T}' = 4.2 \pm 0.1$ (for $K_{0T} = 160.3$ GPa and $V_0 = 11.253$ cm^3/mole). Thus static data

under nearly hydrostatic conditions are also consistent with the ultrasonic and reduced shock data. The volumes predicted by theoretical methods [7,8] differ from the combined shock and ultrasonic equation of state by only 2% or less at pressures near 200 GPa. A third-order Birch-Murnaghan fit to the present static compression data yields $K_{0T} = 177 \pm 4$ GPa and $K_{0T}' = 4.0 \pm 0.1$. This differs markedly from the ultrasonic, shock, and quasihydrostatic compression data (Fig. 2). The ambient-pressure bulk modulus is 10% larger than the ultrasonic value, and the volumes are 1.5% larger at 150 GPa. Other static compression data for MgO under nonhydrostatic stress [20] also yield high bulk moduli ($\sim$180 GPa) and P-V states above the inferred hydrostatic compression curve.

The role of nonhydrostatic stresses in opposed anvil devices has been discussed in detail [1]. The principal stress in the load direction σ_3 is greater than the stress in the radial direction σ_1. In the diamond cell geometry, the incident x-ray beam travels along the load direction and the diffracting plane normals are nearly at right angles to the load axis. Thus diffraction measures strain near the direction of minimum principal stress. The pressure is given by

$$P = \frac{\sigma_3 + 2\sigma_1}{3}, \qquad (1)$$

and, assuming a von Mises yield condition, the shear strength τ is [1]

$$\tau = \tfrac{1}{2}(\sigma_3 - \sigma_1). \qquad (2)$$

A quantitative determination of the shear stresses in our sample may be made in two ways. The first method utilizes the dependence of the lattice parameter on crystallographic direction. The difference in lattice parameters determined from the (220) and (200) MgO lines are shown as a function of pressure in Fig. 2 (inset). With increasing pressure, the lattice parameter from the (220) diffraction line is systematically larger than that from the (200) line by an amount that increases from $\sim$0.1% at 100 GPa to 0.9% above 200 GPa.

From linear elasticity theory, the following expressions describing the lattice strain in a nonhydrostatically compressed cubic sample in the diamond cell can be obtained [1]:

$$\epsilon_m(hkl) = \epsilon_P - \frac{2\tau}{3}(1 - 3\sin^2\theta)$$

$$\times \left[\alpha(S_{11} - S_{12} - 3S\Gamma) + \frac{1-\alpha}{2G_V} \right], \qquad (3)$$

$$\epsilon_m(hkl) = \frac{a_m(hkl) - a_0}{a_0}, \qquad (4)$$

$$S = \frac{S_{44}}{2}(A - 1), \qquad (5)$$

$$\Gamma = \frac{h^2k^2 + k^2l^2 + l^2h^2}{(h^2 + k^2 + l^2)^2}. \qquad (6)$$

Here $\epsilon_m(hkl)$ is the lattice strain (which along with the stress is taken to be negative in compression) and, in general, is a function of the Miller indices hkl of the diffraction plane. $a_m(hkl)$ is the measured lattice parameter for a given (hkl) and a_0 is the ambient-pressure lattice parameter. ϵ_P is the lattice strain produced by the mean normal stress, θ is the scattering angle, and G_V is the Voigt bound on the shear modulus. The parameter α ranges from 0 for conditions corresponding to constant strain across grain boundaries in the sample (Voigt limit) to 1 for continuity of stresses (Reuss limit). The quantity S is a measure of the elastic anisotropy with $A = 2(S_{11} - S_{12})/S_{44}$ and the S_{ij}s being the elastic compliances.

Using (3)–(6), the shear strength of the specimen can be related to the difference in the measured lattice parameters of the (200) and (220) diffraction lines by

$$\tau = \frac{-2[a_m(200) - a_m(220)]}{\alpha a_0 S(1 - 3\sin^2\theta)}. \tag{7}$$

Dependence of the lattice parameter on (hkl) is pronounced in MgO above 100 GPa (Fig. 2, inset). This arises from changes in the product $S\tau$ at high pressures. Assuming $\alpha = 1$ in (7) yields a lower bound to the sample shear strength. S is constrained experimentally to 3 GPa from single-crystal elasticity data [15]. Linear extrapolation of the elastic constants implies a change in the sign of S at about 20 GPa (Fig. 3). This implies that the strongest direction in MgO changes from [111] to [100] at high pressure and the softest direction becomes [111] rather than [100]. We also determine S from elastic constants of MgO to 150 GPa from first-principles model calculations [8] (Fig. 3). While the theoretical calculation overestimates the 1-bar value of S, its initial slope is consistent with the ultrasonic data. The calculated anisotropy reaches zero at about 45 GPa, and becomes increasingly negative at higher pressures. According to (7), the larger lattice parameter from the (220) line relative to the (200)
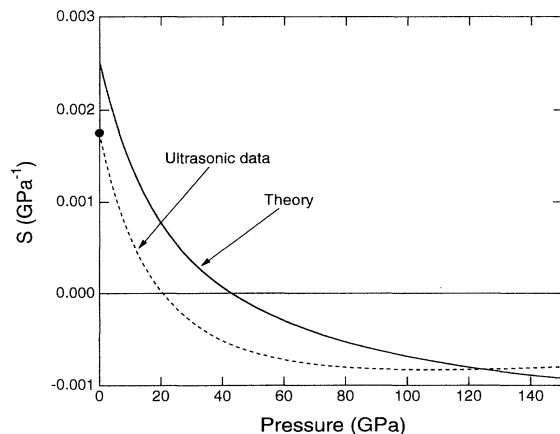
line can only be explained by a negative value of S. This provides direct experimental evidence for a fundamental change in the nature of the elastic anisotropy of MgO at high pressure. A lower bound to the shear strength was determined from the measured difference in the (200) and (220) lattice parameters using the theoretical values for S (Fig. 4). A quadratic fit to the shear strengths determined from the individual data points is shown in the figure. This curve yields a minimum shear strength of 5 GPa at 100 GPa, increasing to at least 11 GPa at the highest pressure (227 GPa).

The second quantitative measure of the sample shear strength can be made from the pressure difference at a given volume achieved under nonhydrostatic and hydrostatic compression. The hydrostat was taken from the fourth-order fit to the combined ultrasonic and shock data (Fig. 2). Assuming the pressure determined from the Mo equation of state represents the mean pressure in the sample and that sample behavior is isotropic, the shear strength is given by [2]

$$\tau = \tfrac{3}{2}(P_{\text{x ray}} - P_{\text{hydrostat}}). \tag{8}$$

The shear stresses calculated by this procedure (Fig. 4) indicate that MgO can sustain increasing shear stresses to at least 100 GPa. Our results are also consistent with static shear strengths determined in earlier, low pressure studies of MgO [5,9,10] (Fig. 4). At higher pressure, we find that shear stresses continue to increase, reaching values of ~ 10 GPa at pressures of 60–100 GPa.

The two methods of shear stress determination yield consistent results. Those obtained using (7) lie below values obtained from pressure offsets, as expected for
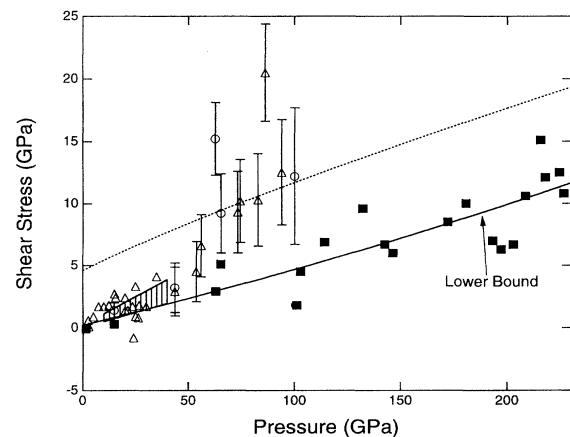
FIG. 4. Shear strength of MgO as a function of pressure. Filled symbols show shear stresses computed from the lattice parameter differences and elastic anisotropy of Figs. 2 and 3. Solid line is a fit to these data. Open symbols (circles—this study, triangles—[20]) show shear stress determinations from pressure offsets of Fig. 2. Data above 100 GPa are not shown because of large uncertainties in volume. The hatched region is from Ref. [10]. The dashed line shows the predicted ideal strength of MgO.

FIG. 3. Elastic anisotropy S as a function of pressure for MgO. The circle is from ambient pressure data, and the dashed line shows the result of linear extrapolation of ultrasonic elasticity data [15]. The solid line is calculated from theory [8].

a lower bound. The large pressure offsets observed at 60–90 GPa and the relatively small difference in lattice parameter at these same pressures can be consistently explained by a material which is nearly elastically isotropic at these pressures, as inferred from the first-principles results. At higher pressures, the difference in lattice parameter increases as a consequence of increased shear stress and/or increased elastic anisotropy. Use of (7) has the important advantage that the shear strength is determined directly from the properties of the sample, and does not rely on an inferred hydrostat or the EOS of a marker material in contact with the sample.

The ideal strength of MgO is approximately 3.5% of the shear modulus [21]. Using the pressure dependence of G from ultrasonic data [15], the MgO shear stresses are compared to this limit in Fig. 4. At 60–90 GPa, the strength of MgO approaches the theoretical limit of the solid. In rhenium, the static strength has been observed to approach 4% of the shear modulus at pressures of ~ 100 GPa [2] which compares to an ideal strength of 5%– 10% of the shear modulus in this material. The shear strength of MgO increases by at least an order of magnitude from ambient pressure to 200 GPa. By characterizing this strength, we find that a single equation of state is consistent with a wide variety of experimental data for this fundamental material. The techniques described here should find wide applicability in the analysis of other ultrahigh pressure diffraction data.

[1] A. K. Singh, J. Appl. Phys. **73**, 4278 (1993).

[2] R. Jeanloz, B. K. Godwal, and C. Meade, Nature (London) **349**, 687 (1991). The terms shear strength and shear stress will be used interchangeably here, although it is recognized that the material shear strength might be larger than our measurements if the maximum shear stress has not been achieved.

[3] Y. K. Vohra, S. J. Duclos, and A. L. Ruoff, Phys. Rev. B **36**, 9790 (1987).

[4] A. K. Singh, High Temp. High Press. **10**, 641 (1978).

[5] G. L. Kinsland, High Temp. High Press. **10**, 627 (1978).

[6] C. Meade and R. Jeanloz, Phys. Rev. B **42**, 2532 (1990); Y. Meng, D. J. Weidner, and Y. Fei, Geophys. Res. Lett. **20**, 1147 (1993); N. Funamori, T. Yagi, and T. Uchida, J. Appl. Phys. **75**, 4327 (1994).

[7] A. J. Cohen and R. G. Gordon, Phys. Rev. B **14**, 4593 (1976); K. J. Chang and M. L. Cohen, Phys. Rev. B **30**, 4774 (1984); M. Causà, R. Dovesi, C. Pisani, and C. Roetti, Phys. Rev. B **33**, 1308 (1986); H. Zhang and M. S. T. Bukowinski, Phys. Rev. B **44**, 2495 (1991).

[8] D. G. Isaak, R. E. Cohen, and M. J. Mehl, J. Geophys. Res. **95**, 7055 (1990).

[9] P. Bridgman, Proc. Am. Acad. Arts Sci. **71**, 387 (1937); M. S. Patterson and C. W. Weaver, J. Am. Ceram. Soc. **53**, 463 (1970); D. J. Weidner, Y. Wang, and M. T. Vaughan, Geophys. Res. Lett. **21**, 753 (1994).

[10] C. Meade and R. Jeanloz, J. Geophys. Res. **93**, 3261 (1988).

[11] J. C. Jamieson, J. N. Fritz, and M. H. Manghnani, in *High Pressure Research in Geophysics*, edited by S. Akimoto and M. H. Manghnani (Center for Academic Publishing, Tokyo, 1982), p. 27.

[12] L. Liu and W. A. Bassett, *Elements, Oxides, and Silicates* (Oxford Univ. Press, New York, 1986).

[13] J. Z. Hu, H. K. Mao, J. Shu, and R. J. Hemley, in *High-Pressure Science and Technology–1993*, edited by S. C. Schmidt, J. W. Shaner, G. A. Samara, and M. Ross (AIP, New York, 1994), p. 441.

[14] R. S. Hixson and J. N. Fritz, J. Appl. Phys. **71**, 1721 (1992).

[15] I. Jackson and H. Niesler, in *High Pressure Research in Geophysics*, Ref. [11], p. 93.

[16] W. J. Carter, S. P. Marsh, J. N. Fritz, and R. G. McQueen, in *Accurate Characterization of the High Pressure Environment*, edited by E. C. Lloyd (NBS, Washington, D.C., 1971), p. 147.

[17] M. S. Vassiliou and T. J. Ahrens, Geophys. Res. Lett. **8**, 729 (1981).

[18] T. S. Duffy and T. J. Ahrens, in *High-Pressure Science and Technology–1993*, Ref. [13], p. 1107.

[19] Y. Fei (unpublished).

[20] E. A. Perez-Albuerne and H. G. Drickamer, J. Chem. Phys. **43**, 1381 (1965); J. S. Weaver, T. Takahashi, and W. A. Bassett, in *Accurate Characterization of the High Pressure Environment*, edited by E. C. Lloyd (NBS, Washington, D.C., 1971), p. 189; H. K. Mao and P. M. Bell, J. Geophys. Res. **84**, 4533 (1979).

[21] H. J. Frost and M. F. Ashby, *Deformation Mechanism Maps* (Pergammon, New York, 1982).